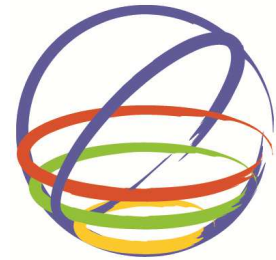


Applicability of Multi-spring Model Based on Finite Strain Theory to Seismic Behavior of Embankment on Liquefiable Sand Deposit



15 WCEE
LISBOA 2012

Kyohei Ueda

Railway Technical Research Institute, Kokubunji, Tokyo, Japan

Susumu Iai & Tetsuo Tobita

Disaster Prevention Research Institute, Kyoto University, Uji, Kyoto, Japan

Osamu Ozutsumi

Meisoshu Co., Toshima-ku, Tokyo, Japan

SUMMARY:

A finite element program “FLIP”, in which a strain space plasticity model called “Multi-spring model” is implemented, has been widely used in seismic design practice in Japan. However, the model is based on the infinitesimal strain theory and the application is limited to small displacement phenomena. Therefore, the authors have extended the model based on finite strain theory including total and updated Lagrangian (TL/UL) formulations and developed a large deformation analysis program, called “FLIP/TULIP”, to simulate large strain and rotation phenomena. This paper presents the applicability of the program by performing seismic response analyses on the dynamic behavior of an embankment in geotechnical centrifuge experiments. Primary conclusions are summarized as follows; (1) Finite strain analyses give closer agreements with measurements than infinitesimal strain analysis does. (2) TL and UL formulations are numerically equivalent. (3) The effect of geometrical nonlinearity has to be considered in predicting the seismic response of embankments.

Keywords: Finite strain analysis, Seismic behavior, Liquefaction, Embankment, Multi-spring model

1. INTRODUCTION

A finite element program “FLIP (Finite Element Analysis of Liquefaction Program)” is a computer program for dynamic effective stress analysis of soil-structure systems during earthquakes including soil liquefaction. The program can simulate residual displacements of soil-structure systems caused by earthquakes, and therefore it has been widely used for seismic performance evaluation and seismic design of urban structures in Japan. In the program, a strain space plasticity model called “Multi-spring model” is implemented as a constitutive model of soil elements. The model can take into account the effect of rotation of principal stress axis directions, the effect of which is known to play an important role in the cyclic behavior of the anisotropically consolidated sand. However, the formulation of the model and governing equations in FLIP have been carried out based on the infinitesimal strain theory, which means that the application should be, strictly speaking, limited to phenomena under small strain, small displacement and small rotation. Although a tentative method called “simplified large deformation analysis” (Ozutsumi, 2003) was introduced into the program in order to overcome the deficit, the method can’t exactly consider the effect of geometrical nonlinearity (as described later). Therefore, the authors have extended the Multi-spring model based on finite strain theory including both total Lagrangian (TL) and updated Lagrangian (UL) formulations to simulate large strain and rotation phenomena. In this research, the performance of the model is studied by simulating the dynamic behavior of embankments on liquefiable sand deposits during shaking in order to verify the applicability of the program.

2. SUMMARY OF CENTRIFUGE MODEL TEST

To study the dynamic behavior of an embankment on a liquefiable sand deposit, a series of centrifuge model tests was performed in the P.W.R.I (2000). The applied centrifugal acceleration was 50 G. In

the experiments, various sorts of countermeasures were adopted. In this research, the target of the simulation is the result of the test case with no countermeasures. A model configuration shown in Fig. 2.1 is a cross section of an embankment on the sand deposit with 13.0 m depth. The crest height is 5.0 m, and lateral length at the top and bottom are 3.0 m and 23.0 m, respectively. Groundwater level is at 1.8 m below the surface of the ground. The relative density of the upper and lower layer of the saturated sand deposit is approximately 60 % and 90 %, respectively. Table 2.1 shows the physical properties of the Edosaki sand, which was used for the upper deposit and embankment, and the silica sand No.7, which was used for the lower deposit. Aggregates were placed at the bottom of the embankment with the aim of preventing the embankment from soaking up pore water by suction. Figure 2.2 shows the input motion, which is composed of seven sinusoidal waves (main shock) with a peak acceleration of approximately 0.4 g and subsequent aftershocks with acceleration amplitudes less than 0.1 g. The induced crest settlement was 2.04 m at the end of the main shocks, and 2.30 m at the end of the aftershocks.

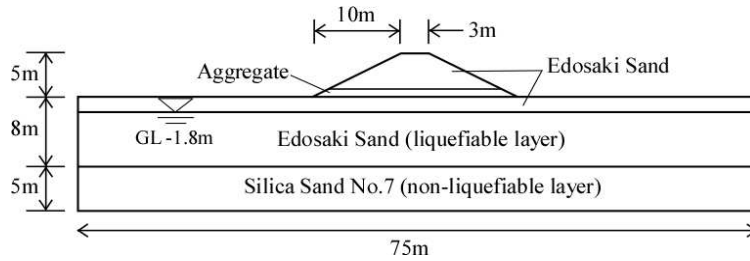


Figure 2.1 Cross-section diagram in centrifuge model test (Modified after P.W.R.I. (2000))

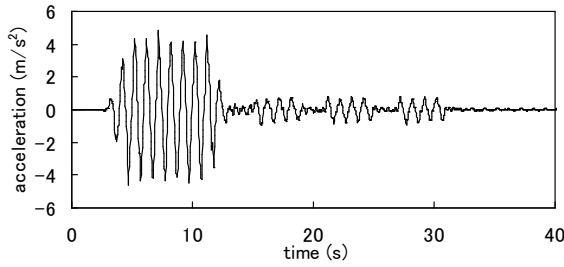


Figure 2.2 Input acceleration (P.W.R.I. (2000))

Table 2.1 Physical Properties of Sands (P.W.R.I. (2000))

	Edosaki Sand	Silica Sand (No.7)
density of sand (g/cm^3)	2.684	2.642
finer content F_c (%)	10.8	0.7
average grain size/diameter D_{50} (mm)	0.181	0.169
relative density D_r (%)	60.7	90.8

3. CONSTITUTIVE MODEL OF SOILS

3.1. Multi-spring Model Based on Infinitesimal Strain Theory

The effective stress model of sands to be used in this study is a strain space multiple mechanism model called “Multi-spring model” (Iai et al., 1992). The model can take into account the effect of rotation of principal stress axis directions, the effect of which is known to play an important role in the cyclic behavior of the anisotropically consolidated sand. Brief summary of the model is given as follows. The integrated form of the constitutive relation is given by

$$\boldsymbol{\sigma}' = \begin{bmatrix} \sigma'_{xx} & \tau_{xy} \\ \tau_{yx} & \sigma'_{yy} \end{bmatrix} = -p\mathbf{I} + \sum_{i=1}^l q^{(i)} \langle \mathbf{t}^{(i)} \otimes \mathbf{n}^{(i)} \rangle \Delta\omega, \text{ where } \langle \mathbf{t} \otimes \mathbf{n} \rangle = \mathbf{t} \otimes \mathbf{n} + \mathbf{n} \otimes \mathbf{t} \quad (3.1)$$

where $p = p(\boldsymbol{\varepsilon}')$ denotes effective confining pressure (isotropic stress), \mathbf{I} indicates second order identity tensor, $q = q(\boldsymbol{\gamma})$ denotes virtual simple shear stress, \mathbf{n} is a unit vector along the direction of the branch between particles in contact with each other, \mathbf{t} is a unit vector normal to \mathbf{n} . The volumetric strain $\boldsymbol{\varepsilon}$ and the virtual simple shear strain $\boldsymbol{\gamma}$ are defined as follows:

$$\boldsymbol{\varepsilon} = \mathbf{I} : \boldsymbol{\varepsilon}, \gamma^{(i)} = \langle \mathbf{t}^{(i)} \otimes \mathbf{n}^{(i)} \rangle : \boldsymbol{\varepsilon}, \text{ where } \boldsymbol{\varepsilon} = \begin{bmatrix} \varepsilon_{xx} & \gamma_{xy} / 2 \\ \gamma_{yx} / 2 & \varepsilon_{yy} \end{bmatrix} \quad (3.2)$$

where the double dot symbol defines double contraction. In order to take into account the effect of volumetric strain due to dilatancy ε_d , effective volumetric strain ε' is introduced by

$$\varepsilon' = \varepsilon - \varepsilon_d, \text{ where } \varepsilon_d = (p_0 S / B)^{1-m_k} - np_0(1-S) / K_f + \varepsilon_0 \quad (3.3)$$

where p_0 and ε_0 indicate the effective confining pressure and volumetric strain at initial state, K_f and n denote the bulk modulus of pore water and the porosity of soil skeleton, m_k is a parameter that controls how the bulk modulus of soil skeleton changes its value depending on confining pressure, S denotes a state variable that determines the location and shape of liquefaction front, and

$$B = p_a \left\{ (1 - m_k) K_{ma} / p_a \right\}^{1/(1-m_k)} \quad (3.4)$$

where p_a is a reference confining pressure and K_{ma} is the bulk modulus of soil skeleton at $p = p_a$. The time derivative of both sides of Equation (3.1) yields the incremental constitutive equation as follows (see Iai et al. (1992) for more details):

$$\dot{\boldsymbol{\sigma}}' = \mathbb{C} : \dot{\boldsymbol{\varepsilon}} \quad (3.5)$$

3.2. Finite Strain Formulation of Multi-spring Model in Reference Configuration

The strain space multiple mechanism model, called ‘‘Multi-spring model’’, under infinitesimal strain theory is to be extended for large deformation analysis based on finite strain formulation. In order to extend the model, first the unit vector \mathbf{N} along the direction of the branch between soil particles and the unit vector \mathbf{T} normal to \mathbf{N} are considered to be defined in the reference configuration of the material. Next, these vectors are assumed to change their direction and magnitude into \mathbf{n} and \mathbf{t} in the current configuration through the deformation gradient \mathbf{F} as follows:

$$\mathbf{n} = \mathbf{F}\mathbf{N}, \mathbf{t} = \mathbf{F}\mathbf{T}, \text{ where } \mathbf{F} = \partial \mathbf{x} / \partial \mathbf{X} \quad (3.6)$$

where \mathbf{X} and \mathbf{x} are the position vector in the reference and current configuration, respectively. The material description of the Multi-spring model in the reference configuration is given as follows with the second Piola-Kirchhoff effective stress \mathbf{S}' :

$$\mathbf{S}' = -Jp\mathbf{C}^{-1} + J^{-1}\mathbb{Q} : \bar{\mathbf{S}}, \text{ where } \mathbf{C} = \mathbf{F}^T\mathbf{F}, J = \det \mathbf{F} \quad (3.7)$$

The fourth-order tensor \mathbb{Q} and the second-order tensor $\bar{\mathbf{S}}$ in Eq. (3.7) are defined by

$$\mathbb{Q} = \mathbb{N} - \mathbf{C}^{-1} \otimes \mathbf{C} / 2, \text{ where } \bar{\mathbf{S}} = \sum_{i=1}^I Jq^{(i)} \langle \mathbf{T}^{(i)} \otimes \mathbf{N}^{(i)} \rangle \Delta \omega \quad (3.8)$$

where \mathbb{N} is the unit fourth-order tensor. Incremental form of the constitutive equation in the reference configuration is derived by taking the material time derivative of both sides of Eq. (3.7) as follows (see Ueda (2009), Iai et al. (2012) for more details):

$$\dot{\mathbf{S}}' = \mathbb{C} : \dot{\mathbf{E}} \quad (3.9)$$

3.3. Finite Strain Formulation of Multi-spring Model in Current Configuration

The spatial description of the Multi-spring model in the current configuration is obtained through the push-forward operation (e.g., Holzapfel, 2001) of the material description in Eq. (3.7) as follows:

$$\boldsymbol{\sigma}' = -p\mathbf{I} + J^{-1}\mathbb{Z} : \bar{\boldsymbol{\sigma}} \quad (3.10)$$

where $\boldsymbol{\sigma}'$ denotes the Cauchy effective stress and

$$\mathbb{Z} = \mathbb{N} - \mathbf{I} \otimes \mathbf{I} / 2, \text{ where } \bar{\boldsymbol{\sigma}} = \sum_{i=1}^I q^{(i)} \langle \mathbf{t}^{(i)} \otimes \mathbf{n}^{(i)} \rangle \Delta \omega \quad (3.11)$$

With the Oldroyd stress rate of the Kirchhoff effective stress (e.g., Holzapfel, 2001), incremental form of the strain space multiple mechanism model in the current configuration is given as follows with the rate of deformation tensor \mathbf{d} (see Ueda (2009), Iai et al. (2012) for more details):

$$\text{Oldr}(J\boldsymbol{\sigma}') = J\mathbb{C} : \mathbf{d} \quad (3.12)$$

4. OUTLINE OF FINITE ELEMENT ANALYSIS

4.1. Determination of Model Parameters

The strain space multiple mechanism model, called “Multi-spring model”, described in the previous chapter has 15 parameters for the analysis considering liquefaction; eight specify volumetric and shear mechanism (deformation characteristics), and the rest controls liquefaction and dilatancy. The parameters for deformation characteristics, which were obtained from the past study (Hyodo et al., 2008), are shown in Table 4.1. The rest parameters for liquefaction and dilatancy, which were determined by referring to the liquefaction resistance curves obtained from the cyclic triaxial tests, are shown in Table 4.2. The parameter q_{us} in Table 4.2, which is the undrained shear strength for describing the steady state of sand, was determined by using a simplified method (Motoshima et al., 2008) from the void ratio and fines content of sands. This parameter is defined only for the Edosaki sand layer, which is considered to have a major effect on the deformation of the embankment, because the fines content of silica sand No. 7 is very small compared to that of Edosaki sand as shown in Table 2.1.

4.2. Initial and Boundary Conditions and Input Motion

Numerical analyses were carried out with the same prototype dimension of the centrifuge model test. Figure 4.1 shows the finite element mesh. In order to approximate the boundary conditions of the rigid container in the model test, degrees of freedom of displacements at the base were fixed both horizontally and vertically, and only horizontal displacements were fixed at the side boundaries. Before dynamic analyses, a static analysis was performed under drained condition with gravity in order to simulate the initial stress condition in the model test before shaking. After the self-weight analysis, a seismic response analysis was performed under the undrained condition by using the recorded motion (Figure 2.2) at the bottom of the container as an input motion. The numerical time integration was done by the Wilson- θ method ($\theta = 1.4$) using a time step of 0.01 seconds. Rayleigh damping ($\alpha=0.0$ and $\beta=0.0002$) was used to ensure stability of the numerical solution process. Selective reduced integration was adopted for Gauss integration using four nodes isoparametric elements. In computation by finite element method, four analytical methods (i.e., infinitesimal strain analysis, simplified large deformation analysis, and finite strain analyses) were performed in order to study about the effect of geometrical nonlinearity on the deformation of embankment. In the finite strain analyses, we employed both TL and UL formulation.

Table 4.1 Model Parameters for Deformation Characteristics

Soil Type	Parameters for deformation characteristics									
	Density	Porosity	Elastic tangent shear modulus	Elastic tangent bulk modulus	Reference mean effective stress	Exponent of power function for modulus		Internal friction angle	Cohesion	Max. damping ratio
	ρ t/m ³	n	G_{ma} kPa	K_{ma} kPa	σ_{ma}' kPa	m_G	m_K	ϕ_f (°)	c kPa	h_{max}
Edosaki Sand (embankment)	1.70	0.49	84000	218000	98.0	0.5	0.5	34.0	0.0	0.26
Edosaki Sand (dry deposit)	1.68	0.49	41000	107000	98.0	0.5	0.5	34.0	0.0	0.26
Edosaki Sand (saturated deposit)	1.86	0.49	41000	107000	98.0	0.5	0.5	34.0	0.0	0.26
Silica Sand No.7 (saturated deposit)	1.98	0.40	86000	224000	98.0	0.5	0.5	48.0	0.0	0.24

Table 4.2 Model Parameters for Dilatancy

Soil Type	Parameters for dilatancy						
	ϕ_p (°)	S_1	w_1	p_1	p_2	c_1	q_{us} (kPa)
Edosaki Sand (saturated)	28.0	0.005	1.80	0.40	0.80	1.70	200.0
Silica Sand No.7 (saturated)	33.0	0.005	2.30	0.30	0.60	2.00	-

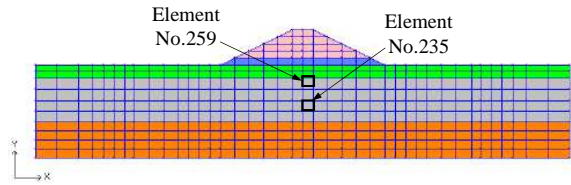


Figure 4.1 Finite element mesh for numerical analysis

4.3. Outline of Simplified Large Deformation Analysis

The Multi-spring model described in the section 3.1 and governing equations (e.g., equation of motion) in FLIP are based on the infinitesimal strain theory, and thereby FLIP program is appropriate for simulating small displacement and small rotation phenomena. However, in practice of seismic response analysis, it is often required to simulate large deformation phenomena. To meet this demand in a swift and practical manner, a tentative method, called “simplified large deformation analysis”, has been introduced in the FLIP program. Brief summary of the method is given as follows.

The equilibrium equation of FLIP program for seismic response analysis is

$$\int_{\Omega} \mathbf{B}^T \hat{\boldsymbol{\sigma}}' dv + \hat{\mathbf{A}} \mathbf{u} + \mathbf{C} \dot{\mathbf{u}} + \mathbf{M} \ddot{\mathbf{u}} = -\ddot{u}_g \mathbf{M} \mathbf{I} + \int_{\Omega} \mathbf{B}^T \hat{\boldsymbol{\sigma}}'_{st} dv, \text{ where } \hat{\mathbf{A}} = \int_{\Omega} \mathbf{B}^T \{ (K_f / n) \hat{\mathbf{m}} \hat{\mathbf{m}}^T \} \mathbf{B} dv \quad (4.1)$$

where \mathbf{B} denotes B matrix, $\hat{\boldsymbol{\sigma}}'$ denotes effective stress vector, \mathbf{u} denotes relative displacement vector of nodes, \mathbf{C} and \mathbf{M} denote damping and mass matrices, \ddot{u}_g denotes input acceleration at the base, \mathbf{I} denotes a matrix for extracting the directional components of excitation from mass matrix, $\hat{\boldsymbol{\sigma}}'_{st}$ denotes initial effective stress vector due to gravity, and K_f denotes bulk modulus of pore water, n denotes porosity, $\hat{\mathbf{m}}$ denotes matrix for extracting the volumetric strain component from the strain vector. As understood from the right hand side of Eq. (4.1), the load terms during seismic response analysis are the inertia due to earthquake motion and the initial stress load term due to gravity. If a deformation is induced in a soil-structure system due to earthquake motions, such as settlements induced in an embankment, the vertical stress in the soil below the structure or embankment will be reduced. In order to capture this phenomenon, self-weight analysis due to gravity are performed using updated coordinates of nodes in accordance with the deformation of the structure at a certain time step interval during seismic response analysis and the results of the self-weight analysis is used to update the initial stress load vector in Eq. (4.1). This analysis is accomplished by the following step by step procedure.

- a) Perform standard self-weight analysis due to gravity.
- b) Perform seismic response analysis for one or specified number of time step(s) by Eq. (4.1).
- c) Update the coordinate of nodes using the relative displacement vector computed by b).
- d) Perform self-weight analysis using the updated coordinate by

$$\int_{\Omega_{new}} \mathbf{B}_{new}^T \hat{\boldsymbol{\sigma}}'_{new} dV = -g \mathbf{M}_{new} \mathbf{I}_v \quad (4.2)$$

where Ω_{new} denotes updated volume for integration of elements, \mathbf{B}_{new} and \mathbf{M}_{new} denote updated B and mass matrices.

- e) $\hat{\boldsymbol{\sigma}}'_{new}$ computed by d) is an updated stress reflecting deformation induced in the structure and this stress should be used for dynamic analysis as nodal force. However, neither B matrix nor element volume for integration in the seismic response analysis is updated. Consequently, the load vector due to gravity for dynamic analysis is computed by using the initial B matrix and initial volume by

$$\int_{\Omega} \mathbf{B}^T \hat{\boldsymbol{\sigma}}'_{new} dV \quad (4.3)$$

- f) Update the second term in the right hand side of Eq. (4.1) with the load vector computed by Eq. (4.3). In this manner, $\hat{\boldsymbol{\sigma}}'_{new}$ is reflected in dynamic analysis. After this step, return to b), and continue the seismic response analysis.

As described above, the equilibrium equations are extended in the simplified large deformation analysis in order to overcome the disadvantage of FLIP program based on the infinitesimal strain theory. However, the formulation of constitutive equations (e.g., Multi-spring model) is the same as that in the infinitesimal strain analysis described in the section 3.1, and therefore the simplified large deformation analysis has some flaws as follows; (1) It requires more computational time than infinitesimal deformation analysis because self-weight analyses are redone many times during a seismic response analysis in certain intervals. (2) It is, in fact, based on infinitesimal strain theory, which means that the effect of geometrical nonlinearity due to large deformation is not accurately considered. (For example, plane elements under rigid body rotation result in inducing some strain variation in the analysis, while no variation of strain (Green-Lagrange strain in a precise sense) components is theoretically induced if the geometrical nonlinearity is appropriately taken into account.) (3) It is not necessarily effective against each and every cross section of soil-structure systems. Considering some disadvantages of the simplified large deformation analysis and the fact that some soil-structure systems have induced settlement and deformation in several meters in past major earthquakes, the conventional FLIP program has a possibility to cause an unacceptable error on engineering judgement by ignoring the effect of geometrical nonlinearity.

5. RESULTS OF THE ANALYSIS

5.1. Computed Deformation of Embankment

Figure 5.1 shows measured and computed deformations of the embankment after shaking. The deformations are shown by deformed meshes in solid lines with reference to the original configuration in broken lines. As shown in Figure 5.1(a), the deformed configuration obtained in the infinitesimal strain analysis differs widely from the measured one shown in Fig. 5.1(e). The deformation shown in Fig. 5.1(a) is unrealistic, in that most part of the embankment sinks down into the liquefiable deposit. Figure 5.1(a) also shows that the infinitesimal strain analysis overestimates the amount of the crest settlement (5.92 m) approximately as 2.6 times as the measurement (2.30 m) at the end of the main shock. By comparing Fig. 5.1(a) and (b), the overestimate of the crest settlement and unrealistic deformed configuration in the infinitesimal strain analysis are improved by performing the simplified

large deformation analysis. The computed amount of the crest settlement is 3.07 m in Fig. 5.1(b), which is about the half of that obtained by the infinitesimal strain analysis and closer to the measured settlement. As mentioned above, the simplified large deformation analysis is very effective for estimating the amount of settlement and deformation of embankments, but has some disadvantages about the computational time and estimate of stress-strain relationship as described in the section 5.4.

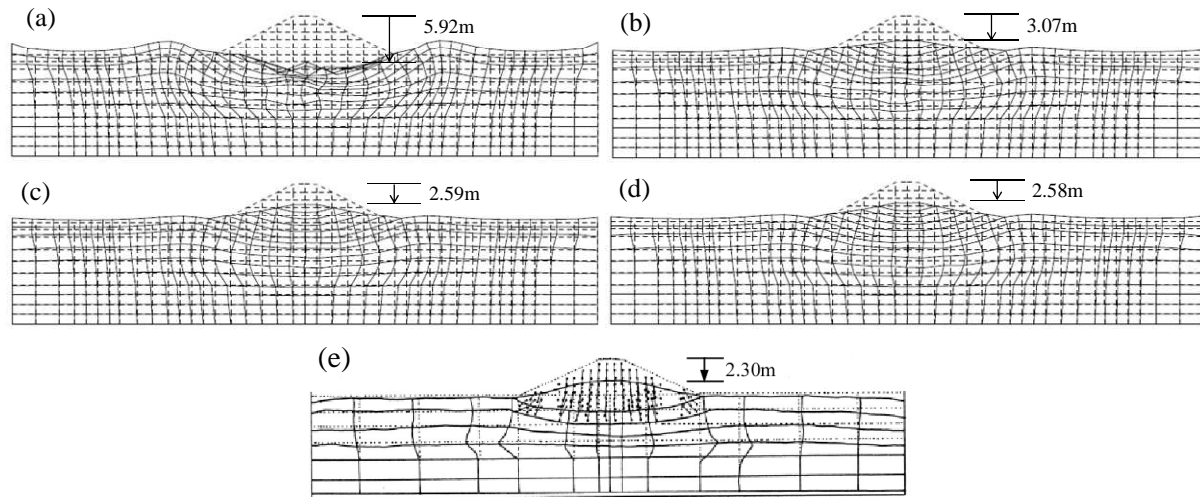


Figure 5.1 Computed and measured deformation: (a) Infinitesimal strain analysis; (b) Simplified large deformation analysis; (c) Finite strain analysis (TL); (d) Finite strain analysis (UL); (e) Centrifuge model test

Figure 5.1(c) and (d) indicate that the results obtained in the finite strain analyses are in good agreement with the measurement shown in Fig. 5.1(e). In both the measurement and computation, soils near toes of the embankment are laterally expanded in the direction opposite to the embankment, while soils under the embankment are compressed vertically and sheared. The computed deformation mode is characterized by a crest settlement associated with lateral spread in foundation soils as the measured one is. The computed deformed configurations show that no significant difference exists between TL and UL formulation. The measured amount of the crest settlement is 2.30 m while the computed ones obtained by using TL and UL formulation are 2.59 m and 2.58 m, respectively, which give close agreement with the measurement and could be considered to be results on a little safer side for design practice. As mentioned earlier about the deformations, both formulations, which are TL and UL formulations, are also equivalent to each other about the settlement. The multiple mechanism model which has been extended based on the finite strain formulation, in which TL or UL formulation could be arbitrarily chosen, shows a reasonable capability to reproduce the deformation and settlement of the embankment.

5.2. Distribution of Excess Pore Water Pressure Ratio

Figure 5.2 shows the computed distribution of excess pore water pressure ratio ($= 1 - \sigma'_m / \sigma'_{m0}$) after shaking. The effect of pore water flow and migration is not considered in the figure because the seismic response analyses are performed under undrained condition. Regardless of the analytical methods (e.g., infinitesimal or large deformation analysis), we can see the fully liquefied zones (i.e. excess pore water pressure ratio is higher than 0.95) of the liquefiable sand deposit near the side boundaries and in the vicinity of the toes of the embankment while the excess pore water pressure ratio in the central zones beneath the embankment generally rises up to only 0.8. This is because soils in the zones constantly undergo the deviator stresses due to overburden stresses from the embankment. These soils tend to undergo shear failure rather than liquefaction. Comparison between Fig. 5.2(a) to (d) indicates that the infinitesimal strain analysis gives a little smaller values of excess pore water pressure ratio in the vicinity of the toes of the embankment and in the central zones beneath the embankment compared to other results. The distribution obtained by the simplified large deformation

analysis shown in Fig. 5.2(b) is generally close to that by the finite strain analyses shown in Fig. 5.2(c) and (d), but they are slightly different in the shallow layer just beneath of the embankment and near the toes of the embankment. For example, at the element No. 259 shown in Fig. 4.2 the excess pore water pressure ratio by the simplified large deformation analysis is about 0.95, which is larger than that by the finite strain analyses (about 0.3). The difference is related to the stress path of the element as described later (see Fig. 5.3(b)). Comparison between Fig. 5.2(c) and (d) shows that TL and UL formulations are equivalent to each other in terms of the distribution of excess pore water pressure ratio as well as the crest settlement.

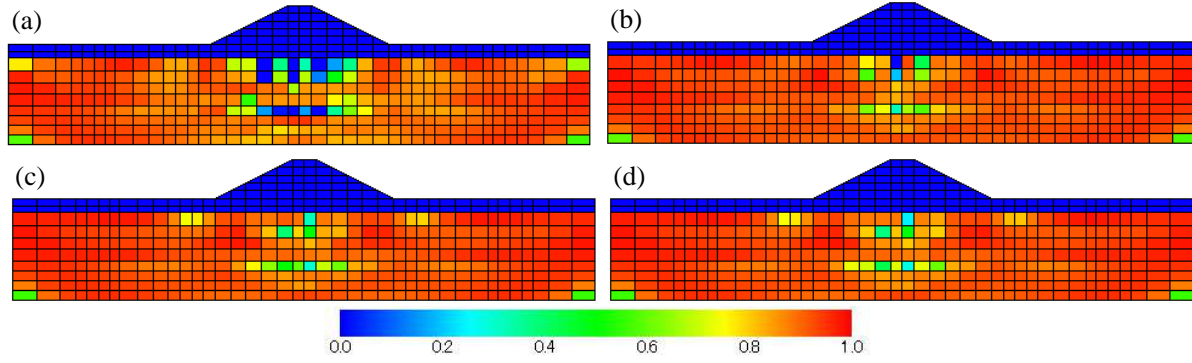


Figure 5.2 Computed distribution of excess pore water pressure ratio after shaking: (a) Infinitesimal strain analysis; (b) Simplified large deformation analysis; (c) Finite strain analysis (TL); (d) Finite strain analysis (UL)

5.3. Effective Stress Path and Stress-strain Relationship

Figure 5.3 shows computed effective stress paths in two elements, which are indicated in Fig. 4.2, beneath the embankment in the liquefiable deposit. In the finite strain analyses, maximum shear stress τ and mean effective stress σ'_m are given by the Cauchy effective stress as follows:

$$\tau = \sqrt{\left(\frac{\sigma'_{11} - \sigma'_{22}}{2}\right)^2 + (\sigma'_{12})^2}, \quad \sigma'_m = (\sigma'_{11} + \sigma'_{22}) / 2 \quad (5.1)$$

Figure 5.3(a) and (b) shows that the effective stress paths with respect to the maximum shear stress in the finite strain analyses are almost consistent with the result in the infinitesimal strain analysis. This consequence indicates the same tendency of the results obtained in simulation for monotonic and cyclic loading (Ueda, 2009). While the stress paths are almost identical at the element No. 235 regardless of the analytical methods as shown in Fig. 5.3(a), at the element No. 259 the stress path obtained by the simplified large deformation analysis is different from other results beyond the phase transformation line and near the failure line as shown in Fig. 5.3(b). This seems to be due to the fact that in the simplified large deformation analysis self-weight analyses are redone with certain intervals during a seismic response analysis in order to take into account the effect of large deformation but the effect of geometrical nonlinearity is not precisely considered.

Computed relationships between shear stress and shear strain for the elements indicated in Fig. 4.2 are shown in Fig. 5.4. In the finite strain analyses, shear stress and shear strain are expressed in terms of the Cauchy (effective) stress and Euler-Almansi strain, respectively. The curves for TL and UL formulations are almost consistent with each other in both Fig. 5.4(a) and (b). Figure 5.4(a) shows that the maximum shear strains in the finite strain analyses are about 10 % while those in the infinitesimal strain analysis and simplified large deformation analysis are 23 %, which is more than twice the results by the finite strain analyses. This is because the effect of geometrical nonlinearity is not precisely considered in the infinitesimal strain analysis and simplified large deformation analysis. The same tendency is shown in Fig. 5.4 (b). As a result, it is necessary to adopt the finite strain analysis in order to take into account the effect of geometrical nonlinearity in seismic response analyses, in particular at the range of shear strain more than 10 %.

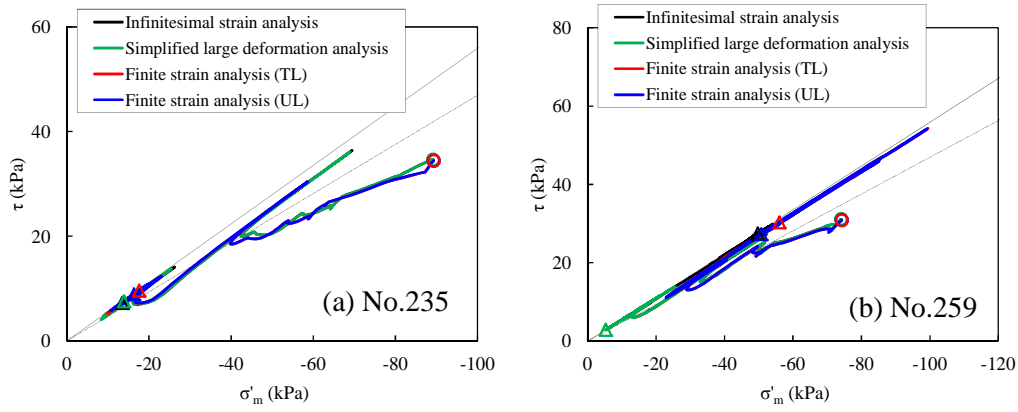


Figure 5.3 Computed effective stress path

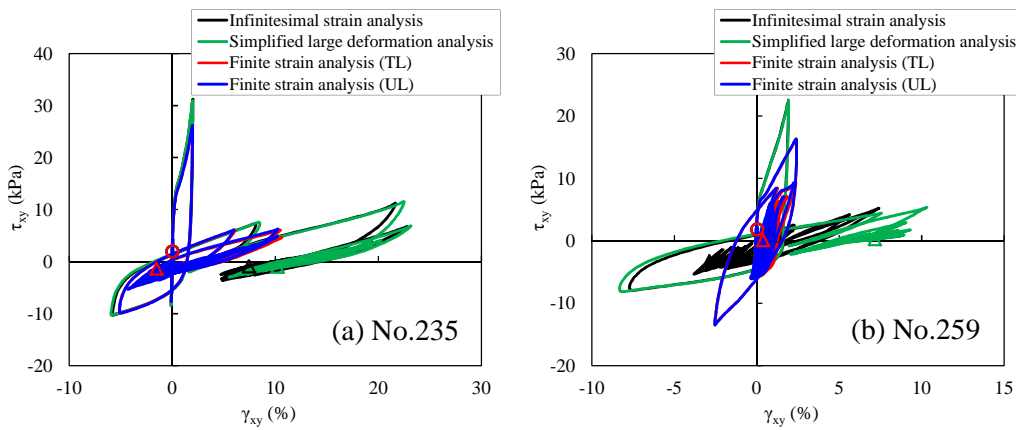


Figure 5.4 Computed relationship between shear stress and shear strain

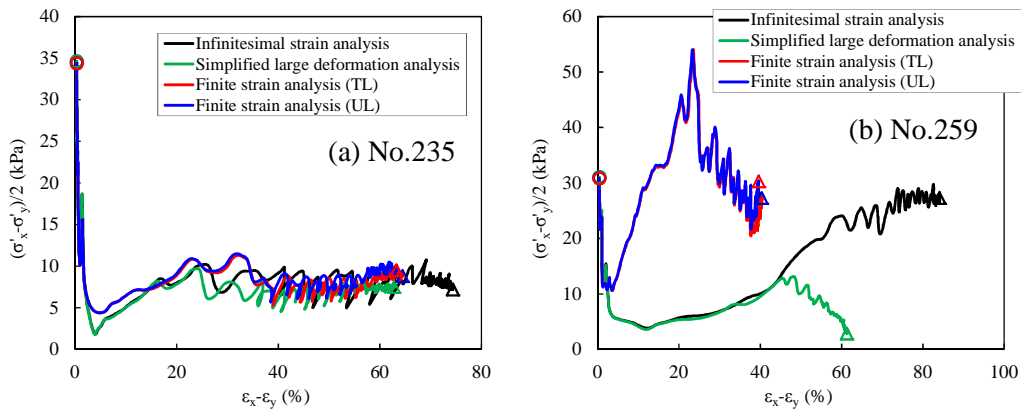


Figure 5.5 Computed relationship between deviator stress and deviator strain

Figure 5.5 shows computed relationships between deviator stress and deviator strain for the elements designated in Fig. 4.2. In the finite strain analyses, deviator stress and deviator strain are expressed by the Cauchy effective stress and the Euler-Almansi strain. As mentioned earlier in Fig. 5.4, the curve in TL formulation gives close agreement with that in UL formulation in both Fig. 5.5(a) and (b). Figure 5.5(a) indicates that significant difference due to the analytical methods is not recognized. In contrast, the infinitesimal strain analysis and simplified large deformation analysis overestimate the residual deviator strain approximately as twice and 1.5 times, respectively, as those in the finite strain analyses as shown in Fig. 5.5(b). This means that the simplified large deformation analysis can't take into account the effect of geometrical nonlinearity appropriately as well as the infinitesimal strain analysis because the both analytical methods are based on infinitesimal strain theory. So, when the range of

large strain as shown in Fig. 5.5 is targeted, it is desirable to perform the finite strain analysis based on finite strain formulation rather than the simplified large deformation analysis.

6. CONCLUSION

In this study, simplified large deformation and finite strain analyses are performed in addition to infinitesimal strain analysis on the dynamic behavior of an embankment on liquefiable sand deposit in geotechnical centrifuge experiments in order to verify the applicability of an effective stress model. The model used in the analysis is a strain space multiple mechanism model called “Multi-spring model”, which has been extended based on finite strain formulation to take into account the effect of geometrical nonlinearity. Primary conclusions of this study are summarized as follows:

The computed crest settlements of the embankment after shaking in the simplified large deformation and finite strain analyses give close agreement with the measured one, while the infinitesimal strain analysis overestimates the measurement. Comparison of the former two analytical methods indicates that the finite strain analyses possess higher accuracy than the simplified large deformation analysis for estimating the crest settlement of embankments. In the infinitesimal strain analysis, the deformed configuration, in which most parts of the embankment sink down into the liquefiable deposit, is widely different from the observed deformation. On the contrary, the simplified large deformation and finite strain analyses well simulate the observed deformed configuration.

The computed stress-strain relationships by the simplified large deformation analysis indicates that the analytical method can't take into account the effect of geometrical nonlinearity appropriately because it is based on the infinitesimal strain theory. Thereby, when large deformation phenomena such as settlement of embankments are considered, it is desirable to perform the finite strain analysis based on the finite strain formulation rather than the simplified large deformation analysis. All of the computed results (e.g., crest settlement, stress-strain relationship) indicate that the total and updated Lagrangian formulations are not only theoretically but also numerically equivalent to each other, and therefore demonstrate the validity of the computer programming for finite strain analysis.

ACKNOWLEDGEMENT

The authors would like to thank the members of the FLIP consortium (http://www.flip.or.jp/flip_english.html) for providing some analytical input data (e.g., the finite element mesh and input wave) to carry out this study.

REFERENCES

- Holzapfel, G.A. (2001). *Nonlinear Solid Mechanics*, John Wiley&Sons.
- Hyodo, J., Iai, S., Yokoyama, N., Ozutsumi, O., and Yoshikawa, S. (2008). Effective Stress Analysis Considering Steady State of Sandy Soil on Centrifuge Model Test. The 43rd Japan National Conference on Geotechnical Engineering, 1807 -1808 (in Japanese).
- Iai, S., Matsunaga, Y., and Kameoka, T. (1992). Strain Space Plasticity Model for Cyclic Mobility. *Soils and Foundations*. **32**: 2, 1-15.
- Iai,S., Ueda,K., Tobita,T. and Ozutsumi,O. (2012). Finite Strain Formulation of a Strain Space Multiple Mechanism Model for Granular Materials. *IJNAMG* (in print) early view (on-line published) as nag2084.
- Motoshima, K., Iai, S., Yokoyama, N., and Sawada, S. (2008). Influence of Fine Fraction Content, Void Ratio, etc. to the Steady State of Sandy Soil. The 43rd Japan National Conference on Geotechnical Engineering, 1799 -1800 (in Japanese).
- Ozutsumi, O. (2003). Study on Numerical Methods for Estimating Earthquake Induced Damage of Soil-structure System on Liquefiable Ground. Doctoral Thesis. Kyoto University. Japan (in Japanese).
- Public Works Research Institute (2000). An Experimental Study on the Effects of Remedial Measure for Embankment Failure due to Earthquake-induced Foundation Liquefaction. Technical Note of P.W.R.I. No.3688 (in Japanese).
- Ueda, K. (2009). Finite Strain Formulation of a Strain Space Multiple Mechanism Model for Granular Materials and its application. Doctoral Thesis. Kyoto University. Japan (in Japanese).